




Cite this: *Polym. Chem.*, 2024, **15**, 5023

## Effect of molar mass of poly(2-oxazoline) based glycopolymers on lectin binding†

Caitlin L. A. Nutting, James Lefley, Zivani Varanaraja, Gokhan Yilmaz and C. Remzi Becer \*

Glycopolymers are a versatile polymer type employed in many applications, especially the biomedical field, due to their ability to exploit multivalent lectin–carbohydrate interactions. Understanding how to improve and manipulate the interactions between glycopolymers and lectins is crucial for their success within the pharmaceutical industry. Herein, we synthesised block copolymers *via* cationic ring opening polymerisation of 2-ethyl-2-oxazoline and 2-(3-butenyl-2-oxazoline) with varying quantities of 2-ethyl-2-oxazoline. These polymers were further functionalised with pendent glucose moieties to produce glycopolymers. All polymers and glycopolymers were analysed using a variety of techniques including NMR, GPC, FT-IR and MALDI-ToF MS. Their binding capabilities were evaluated by surface plasmon resonance, utilising human lectins: DC-SIGN, MBL and Langerin, to investigate how the molar mass influences lectin binding.

Received 9th October 2024,  
Accepted 12th November 2024

DOI: 10.1039/d4py01135j

rsc.li/polymers

### Introduction

Over the last decade, glycopolymers have gained significant attention due to their ability to mimic naturally occurring carbohydrate containing macromolecules which are able to bind to lectins.<sup>1,2</sup> Lectins are crucial proteins within the body, mediating attachment and binding of carbohydrate containing molecules, allowing for their pivotal role in executing recognition events.<sup>3,4</sup> This is essential for biological processes including modulating the inflammatory response,<sup>5</sup> pathogen elimination,<sup>6</sup> and regulation of glycoproteins.<sup>7</sup>

The ability of glycopolymers to bind to lectins enables them to prevent bacterial infiltration,<sup>8</sup> adhesion,<sup>9</sup> and biofilm formation.<sup>10,11</sup> Consequently, various biomedical applications have been developed including drug delivery systems,<sup>12</sup> gene delivery,<sup>13,14</sup> disease inhibition,<sup>15</sup> and biosensors.<sup>16–19</sup> However, development has often been hindered by their limited specificity towards targeted lectin sites, toxicity and bioavailability.<sup>1,10</sup> The increased attention towards lectin binding glycopolymers, with their advantageous multivalency characteristics, has led to more research and in turn a greater understanding of specific site binding *via* the control of chemical characteristics, topology and morphology.<sup>20–25</sup> These features can be modified and adapted to a specific site by manipulating the length of the glycopolymer,<sup>15</sup> backbone

rigidity and flexibility,<sup>26,27</sup> molecular weight,<sup>28</sup> and polymeric chain architecture.<sup>29,30</sup>

Poly (2-oxazoline)s (POx) are an upcoming class of biomaterials that are being recognised as promising alternatives to poly(ethylene glycol) (PEG) because of their tuneability, biocompatibility and reduced cytotoxicity.<sup>31,32</sup> POx first gained attention in the biomedical field when Zalipsky *et al.*<sup>33</sup> highlighted the impressive pharmacokinetics of poly(2-ethyl-2-oxazoline) (PEtOx). POx is synthesised *via* cationic ring opening polymerisation (CROP), a living polymerisation technique. POx exhibits well-defined polymers with narrow dispersion and controlled architecture<sup>34</sup> that are highly tuneable<sup>35</sup> and have high end-group fidelity.<sup>36</sup> Additionally, POx have shown to be more tuneable with a greater array of monomers,<sup>37</sup> enhanced ‘stealth’ like properties,<sup>31</sup> and good solubility in various common solvents.<sup>38</sup> This addresses concerns associated with PEG and PEGylated drugs.<sup>39</sup> Presently, PEtOx based drugs and drug delivery systems are being investigated with one going through a clinical trial for Parkinson’s disease.<sup>40</sup>

Molar mass is a tuneable feature of glycopolymers. The glycopolymer length and make up can lead to interesting morphological and chemical features. These have been previously investigated specifically in self-assembly and how glycopolymers can self-assemble into micelles,<sup>41</sup> polymersomes,<sup>42</sup> and other diverse structures. Molar mass has previously been evaluated by increasing both the polymer chain length and pendent carbohydrate moieties,<sup>28,43,44</sup> or by how the polymer chain length influences cellular uptake.<sup>45</sup> It has been found that there is a maximum point for increasing the glycopolymer multivalency, likely due to either all available binding sites

Department of Chemistry, University of Warwick, Coventry, CV4 7AL, UK.

E-mail: remzi.becer@warwick.ac.uk

† Electronic supplementary information (ESI) available. See DOI: <https://doi.org/10.1039/d4py01135j>



being occupied, or coiling of the polymer backbone.<sup>46</sup> However, it has never been investigated and distinguished whether the binding is enhanced or diminished by the glycopolymer chain length, molar mass or increasing amount of carbohydrate groups.

Herein, we evaluate how increasing the molar mass of glycopolymers, whilst keeping the carbohydrate content constant, affects the lectin binding capabilities. The glycopolymers (GP1–GP5), composed of a fixed block length of 2-(3-butenyl-2-oxazoline) (ButeneOx), and varying block length of EtOx were synthesised *via* CROP. Thiol–ene click chemistry was utilised for the post-polymerisation modification of PButeneOx to yield glycopolymers GP1–GP5, (Scheme 1). Thus, we were able to synthesise a small set of glycopolymers with varying molar mass from 7100 to 14 700 Da. From this, the binding capabilities were evaluated *via* surface plasmon resonance (SPR) with the biologically relevant human lectins mannose binding lectin (MBL), dendritic cell-specific intercellular adhesion molecule-3-grabbing non-integrin (DC-SIGN) and Langerin.

## Experimental

### Materials

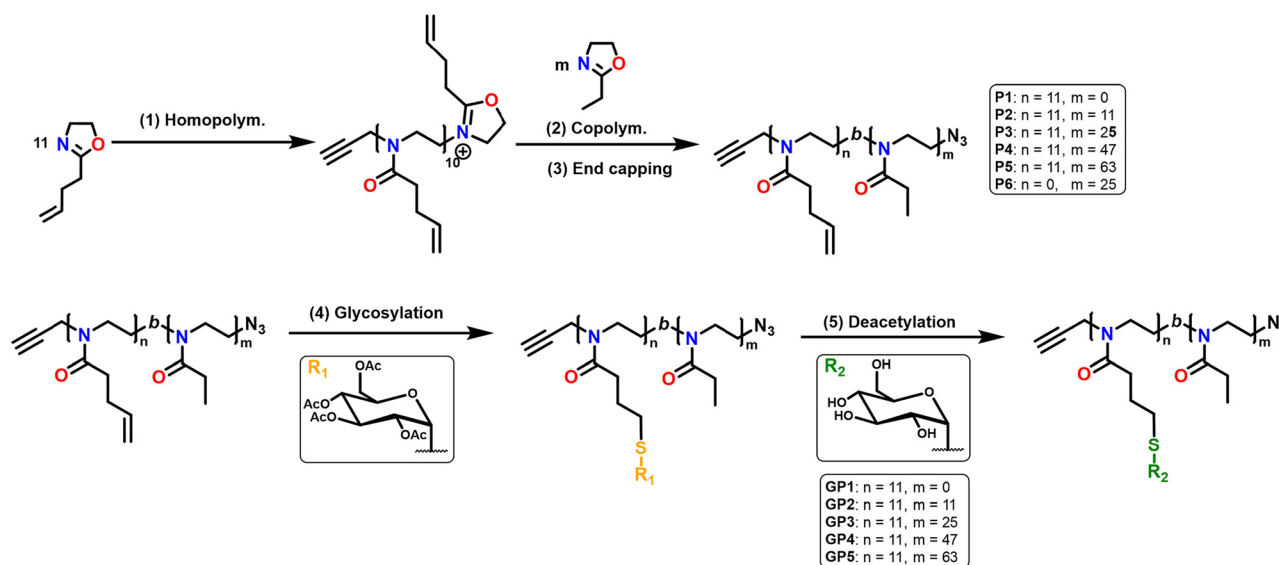
4-Pentenoic acid (Merck; 98%), *N*-hydroxysuccinamide (NHS) (Aldrich, 98%), 1-ethyl-3-(3-dimethylaminopropyl)carbodiimide (EDAC) (ABCRC; 98%), 2-chloroethylamine (Alfa Aesar; 98%), triethylamine (TEA) (Merck; 99%), potassium hydroxide (KOH) (Aldrich; ≥85%), sodium azide (NaN<sub>3</sub>) (Aldrich;

≥99.5%), β-thioglucose tetraacetate (Fisher Scientific; 97%), sodium methoxide solution (25% w/t in methanol) (Aldrich, 95%), dimethyl 2,2'-azobis(2-methylpropionate) (V601) (Fujifilm; 97%), anhydrous acetonitrile (Extra Dry) (Fisher Scientific; ≥99%), dichloromethane (DCM) (Aldrich, ≥99%), tetrahydrofuran (THF) (Aldrich, ≥99%), dimethylformamide (DMF) (Aldrich, ≥99%), methanol (MeOH) (Aldrich, ≥99%), were all purchased and were used as received. Both 2-ethyl-2-oxazoline (EtOx) (Fisher Scientific; 99%) and propargyl *p*-toluenesulphonate (propargyl tosylate) (Fisher Scientific; 98%) were distilled over calcium hydride (CaH<sub>2</sub>) (Aldrich; for synthesis) and then stored under nitrogen. All moisture sensitive reactions were carried out under nitrogen. All lectins were purchased from Biotechne – R&D Systems.

### Analytical techniques

**Nuclear magnetic resonance (NMR)** spectra were recorded on a Bruker Avance III AV 400 MHz at 278 K. Analysis was carried out in CDCl<sub>3</sub> or D<sub>2</sub>O and the residual peak from CHCl<sub>3</sub> and H<sub>2</sub>O were used as the reference chemical shift. The data analysis was performed using TopSpin 4.1.1 Software.

**Gel permeation chromatography (GPC)** measurements were performed using THF (2% TEA and 0.1% BHT) as the eluent. The Agilent Technologies 1260 Infinity instrument was equipped with a refractive index (RI) and 308 nm UV detector, a PLgel 5 μM guard column, and a PLgel 5 μM mixed D column (300 × 7.5 mm). Samples were run at 1 mL min<sup>-1</sup> at 40 °C. Poly(methyl methacrylate) (PMMA) standards (Agilent



**Scheme 1** Overall scheme of the synthesis of the thio-glucose-functionalised PEtOx-*b*-PButeneOx glycopolymers forming GP1–GP5. **Step 1.** Cationic ring opening polymerisation of ButeneOx, which is initiated by propargyl *p*-toluenesulphonate (1 equiv.) in acetonitrile (4 M, 110 °C) and reacted for 22 minutes. **Step 2.** The addition of the second EtOx block in varying amounts which was then subsequently left to polymerise for the appropriate amount of time at 110 °C to obtain P1–P6. **Step 3.** The copolymers are subsequently terminated with sodium azide (NaN<sub>3</sub>) (3 equiv.). After being left to stir for 24 hours, the resulting polymers are precipitated into diethyl ether and dried under vacuum. **Step 4.** Radical mediated thiol–ene click reaction using β-thioglucose tetraacetate (1.2 equiv. per double bond) and dimethyl 2,2'-azobis(2-methylpropionate) (V601) (0.25 equiv.) in tetrahydrofuran (THF) (7 μM, 70 °C) obtaining the acetylated analogues of GP1–GP5. **Step 5.** Deprotection of the thio-glucose tetraacetate using sodium methoxide (NaOMe) (22 equiv.) in methanol (MeOH) (0.016 M) to yield the final glycopolymers GP1–GP5.



PMMA calibration kits M-M-10 and M-L-10) were used for the calibration. All polymer samples were made up to 1 mg mL<sup>-1</sup> using THF and then before injection (100 μL), the samples were filtered through a PTFE membrane with a 0.2 μL pore size. Experimental molar mass ( $M_n$ ), weight-average molar mass ( $M_w$ ), and dispersity ( $\mathcal{D}$ ) values of synthesised polymers were determined by conventional calibration using Agilent GPC/SEC software. GPC measurements in dimethylformamide (DMF) were carried out on an Agilent 1260 Infinity II instrument with two Polargel M columns and a Polargel M guard column. The mobile phase was DMF stabilised with 0.1% w/v lithium bromide (LiBr) with a flow rate of 1 mL min<sup>-1</sup> at a 50 °C and equipped with the following detectors: differential refractive index (DRI), viscometer (VS), light scattering (LS), and variable wavelength detector (MWD). Agilent poly(methyl methacrylate) Easivials were used to create a third order calibration curve. The calibrants cover a range between 535 and 538 500 g mol<sup>-1</sup>. All glycopolymer samples were made up to 1 mg mL<sup>-1</sup> using DMF and were then passed through 0.2 μm nylon filters prior to GPC measurements. All samples were then analysed using Agilent GPC/SEC software.

**Matrix-assisted laser desorption ionization-time-of-flight mass spectrometry (MALDI-ToF MS).** MALDI-ToF MS was performed on a Bruker Daltonics Autoflex spectrometer equipped with a nitrogen laser at 337 nm with positive ion detection. Polymer samples were prepared as follows: solutions in THF of *trans*-2-[3-(4-*tert*-butylphenyl)-2-methyl-2-propenylidene] malononitrile (DCTB, ≥98%) as matrix (20 mg mL<sup>-1</sup>), sodium trifluoroacetate (NaTFA) as cationization agent (10 mg mL<sup>-1</sup>), and sample (5 mg mL<sup>-1</sup>) were mixed in a ratio of 5 : 2 : 5 and then spotted onto the target (0.5 μL). Spectra were recorded in reflective mode, and the mass spectrometer was calibrated with a PMMA standard up to 3 kDa.

**Surface plasmon resonance (SPR).** SPR was used for interaction analysis for all lectins. The extent of interaction between the glycopolymers and lectins were analysed on a BIAcore T200 system (Cytiva Life Sciences). The lectins (0.005 mg mL<sup>-1</sup>) were immobilized *via* a standard amino coupling protocol onto a CM5 sensor chip that was activated by flowing a 1 : 1 mixture of 0.1 M *N*-hydroxy succinimide and 0.05 M *N*-ethyl-*N'*-(dimethylamino propyl) carbodiimide over the chip for 5 min at 25 °C at a flow rate of 10 μL min<sup>-1</sup> after the system equilibration with HEPES filtered buffer (10 mM HEPES pH 7.4, 150 mM NaCl, 5 mM CaCl<sub>2</sub>). Subsequently, channels 1 (blank), 2, 3, and 4 were blocked by flowing a solution of ethanol amine (1 M pH 8.5) for 10 min at 10 μL min<sup>-1</sup> to block the remaining reactive groups on the channels. Sample solutions were prepared at varying concentrations (20.0–1.25 μM) in the same HEPES buffer to calculate the binding kinetics. Sensorgrams for each glycopolymer concentration were recorded with a 350 seconds injection of polymer solution (on period), followed by 200 seconds of buffer alone (off period). Regeneration of the sensor chip surfaces was performed using 10 mM HEPES pH 7.4, 150 mM NaCl, 10 mM EDTA, and 0.01% Tween20 surfactant solution. A blank analyte was also used to correct for unspecific binding events.

Kinetic data was evaluated using a single set of sites (1 : 1 Langmuir binding model) in the BIA evaluation 3.1 software.

**Dynamic light scattering (DLS)** measurements were carried out on an Anton Paar Litesizer instrument using a disposable cuvette. Samples were measured at 25 °C at a backscattering measuring angle of 175°. Each sample was measured in triplicate with 30 runs per measurement and 5 min equilibration time between each measurement. PEO refractive index used was 1.52.

**Transmission electron microscopy (TEM).** Nanostructure solutions were imaged after a negative staining treatment. The samples were drop-cast on glow discharged 300 mesh carbon-coated copper TEM grids (Agar Scientific, Stansted, U.K.). After 3 min incubation, excess solution was removed by blotting with filter paper before incubation with 0.75% phosphotungstic acid solution for 1 min. Excess stain was removed by blotting with filter paper and dried under a vacuum before imaging. Bright-field TEM imaging was performed on a JEOL 2100 Plus Transmission Electron Microscope operated at an acceleration voltage of 200 keV. All the images were recorded on a Gatan Orius 11 megapixel digital camera, and at least six areas were analysed.

#### Fourier transform infrared spectroscopy (FT-IR)

FT-IR was carried out on Agilent Cary 630 with ATR sampling module running at 65 scans per sample with a speed of 0.5 cm s<sup>-1</sup>.

**Synthesis of 2-(3-butenyl-2-oxazoline) ButeneOx.** ButeneOx was synthesised *via* a 3-step synthesis adapted from literature.<sup>47</sup> **Step 1** 4-pentenoic acid (0.38 mol, 1 equiv.), NHS (1.6 equiv.) and EDAC (1.2 equiv.) were dissolved in dichloromethane (DCM) (200 mL) and stirred at 0 °C for 24 h. The solution was washed with water (6 × 100 mL) and then brine (2 × 100 mL). The organic layers were combined and dried over magnesium sulphate (MgSO<sub>4</sub>). DCM was removed *via* rotary evaporation yielding product A (yellow liquid, 66 g) (Fig. S1†).

**Step 2** Product A was combined with 2-chloroethylamine hydrochloride (0.33 mol, 1 equiv.) and dissolved in DCM (150 mL). Triethylamine (TEA) (2.5 equiv.) was added dropwise to the reacting mixture which was stirred at 0 °C for 24 h. The solution was washed with water (6 × 100 mL) and then dried over MgSO<sub>4</sub>. The DCM was removed *via* rotary evaporation to yield product B (yellow liquid, 38 g, Fig. S2†). **Step 3** Potassium hydroxide (KOH) (0.23 mol, 1 equiv.) was dissolved in methanol (MeOH) (135 mL) and added dropwise to product B and was then stirred at 50 °C for 24 h. The product was then filtered and MeOH was removed *via* rotary evaporation. The liquid was distilled twice. The first distillation was carried out under vacuum and the distillate was observed at 30 °C. This was then subsequently stirred with calcium hydride (CaH<sub>2</sub>) for 24 h and distilled a second time under vacuum and the distillate was observed at 30 °C. The system was then sparged under nitrogen to yield 2-(3-butenyl-2-oxazoline) (clear liquid, 12 g, Fig. S3†).

**Synthesis of poly(2-(3-butenyl)-2-oxazoline)<sub>11</sub> P1.** To a dried, nitrogen sparged microwave vial, ButeneOx (11 equiv.),



acetonitrile (4 M) and propargyl tosylate (1 equiv.) were combined to form a stock solution. The appropriate calculated amount was extracted and removed to a separate vial which was then placed in an oil bath at 110 °C for 22 minutes. The cap was then removed, and sodium azide added (3 equiv.). The vial was then resealed and left to return to room temperature overnight. The polymer was then purified by filtering and precipitating into diethyl ether, the sample was dissolved with small amounts of THF. This was then centrifuged and the solvent removed under vacuum to yield a white solid.

**Synthesis of poly(2-(3-buteneyl)-2-oxazoline)<sub>n</sub>-b-poly(2-ethyl-2-oxazoline)<sub>m</sub> P2–P5.** To a dried, nitrogen sparged microwave vial ButeneOx (11 equiv.), acetonitrile (4 M) and propargyl tosylate (1 equiv.) were combined to form a stock solution. The appropriate calculated amount was extracted and removed to a separate vial which was then placed in an oil bath at 110 °C for 22 minutes. EtOx was subsequently added in varying ratios and left for an appropriate time (Table 1). The cap was removed, and sodium azide added (3 equiv.). The vial was then resealed and left to return to room temperature overnight. The polymer was then purified by filtering and then precipitating into diethyl ether, the sample was dissolved with small amounts of THF. This was subsequently centrifuged and then the solvent removed under vacuum to yield a white solid.

**Glycosylation of polymers P(ButeneOx) and P(ButeneOx)-b-P(EtOx) P1–P5.** Each polymer was dissolved in THF (4 mL) with β-thioglucose tetracetate (1.2 equiv. per double bond) and then a stock solution of V601, prepared in THF, the appropriate amount (1 mL) (0.25 equiv. per double bond) was extracted and added to the vial which was left to degas with nitrogen for 30 min. The vial was then placed in an oil bath at 70 °C for 24 hours. This process was monitored by <sup>1</sup>H NMR and repeated until all the double bonds disappeared. The THF was subsequently removed *via* rotary evaporation.

**Deacetylation of glycopolymers GP1–GP5.** Each glycopolymer was dissolved in MeOH (0.016 M, 27 mL) and NaOMe (46.5 mg, 22 equiv.) was added. The mixture was left to stir at

room temperature for 24 hours. The solvent was removed under reduced pressure and the product dissolved in water (~2 mL). The resulting crude solution was then transferred into a dialysis bag (MWCO: 1 kDa) and dialyzed against water for 3 days. Lyophilization produced the final glycopolymers GP1–GP5 (white solid).

## Results and discussion

### Synthesis and analysis of block copolymerisation *via* CROP

Non-functionalised block copolymers P1–P6 were synthesised *via* CROP using a one-pot, sequential addition method utilising propargyl tosylate as an initiator and sodium azide as the terminating agent. Optimal conditions for the copolymerisation between PButeneOx and PEtOx were implemented from a previous study carried out by Schlaad *et al.*,<sup>47</sup> with the homopolymerisation conditions of PButeneOx confirmed *via* a kinetic study (Fig. S4†). The first block was kept the same throughout the series *via* a stock solution of ButeneOx, keeping the [M]/[I] ratio = 11 (Fig. S5†). The conversion of the first block was confirmed *via* <sup>1</sup>H NMR and GPC. Subsequently, the second block was then added in varying [M]/[I] ratios, ranging from 9 to 63. The purified polymers were then analysed by GPC and <sup>1</sup>H NMR (Table 1, Fig. 1(A)–2, Fig. S6–S10 and S11–18†). MALDI-ToF was used to demonstrate the end group fidelity of P1 (Fig. S11†). All polymers achieved ≥99% monomer conversion apart from P6 which achieved 97%. This was confirmed by the lack of monomer present in the final <sup>1</sup>H NMR (Fig. 2), usually observed in the region of ~4.2 ppm and ~3.7 ppm. Polymers P1–P5 showed a slight difference between  $M_{n, \text{theo}}$  (calculated from conversion) and  $M_{n, \text{GPC}}$  (Table 2). Polymers P1–P5  $M_{n, \text{theo}}$  (calculated from conversion) and  $M_{n, \text{GPC}}$  matched up well. High dispersity was shown in the larger blocks P4 and P5, this is likely attributed to early termination after the addition of the second block. This monomer combination has been selected due their water solubility and ability to undergo post-polymerisation functionalisation, making it a good starting point for future biomedical applications. Block

**Table 1** A Summary table of the homopolymers and block copolymers of PEtOx and PButeneOx. All polymers reached greater than 99% conversion except P6 which reached 97% conversion

Code	PButeneOx (DP)	PEtOx (DP)	$M_n$ (theo) (Da)	$M_n$ (GPC) (Da)	$D$
P1	11	0	1500	1800 <sup>a</sup>	1.42
P2	11	9	2300	2500 <sup>a</sup>	1.32
P3	11	25	3900	3900 <sup>a</sup>	1.35
P4	11	45	5900	5900 <sup>a</sup>	1.68
P5	11	63	7700	7800 <sup>a</sup>	1.50
P6	0	30	3000	2800 <sup>a</sup>	1.16
GP1	11	0	4000	7100 <sup>b</sup>	1.29
GP2	11	9	4700	8700 <sup>b</sup>	1.21
GP3	11	25	6300	9500 <sup>b</sup>	1.24
GP4	11	45	8300	13000 <sup>b</sup>	1.27
GP5	11	63	10 100	14700 <sup>b</sup>	1.17

<sup>a</sup> GPC analysis of polymers was performed using eluent: THF +2% TEA +0.1% BHT. <sup>b</sup> GPC SEC analysis of glycopolymers were performed using eluent: DMF +0.1% LiBr.

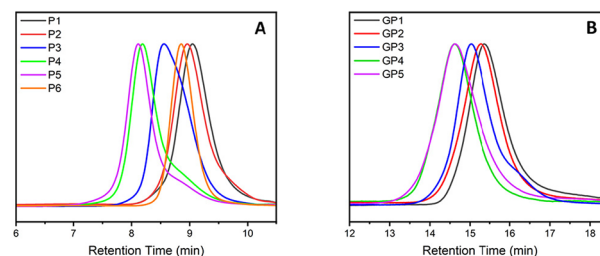


**Fig. 1** (A) GPC traces of PButeneOx with varying amounts of PEtOx: P1–P5. Measurements performed using THF (+2% TEA and +0.1% BHT) as the eluent. PMMA standards were used for calibration. (B) GPC traces of PButeneOx with varying amounts of PEtOx: GP1–GP5. Measurements performed using DMF (+0.1% LiBr) as the eluent. PMMA standards were used for calibration.



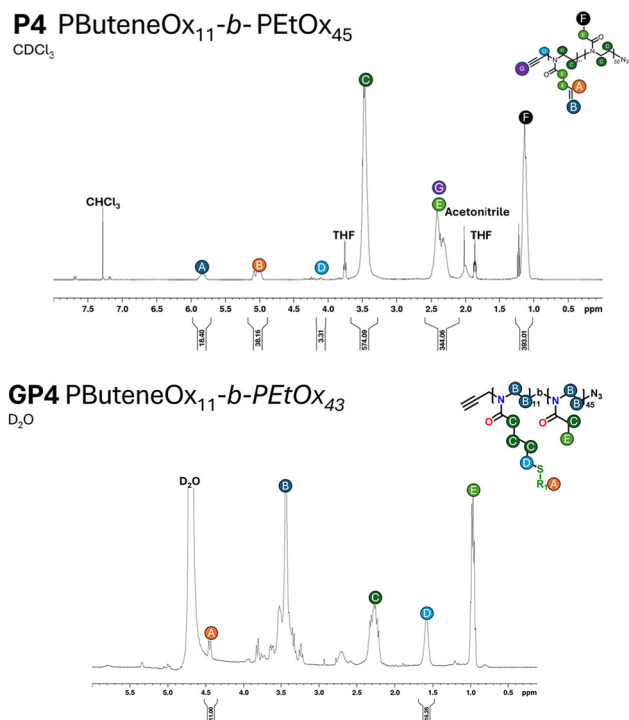


**Fig. 2** A representative example of the  $^1\text{H}$  NMR of the polymer and glycopolymer of **P4** and **GP4**. All measurements were performed on an AV400 MHz NMR.

**Table 2** Kinetic data of binding between glycopolymers (**GP1–GP5**) and lectins (DC-SIGN, MBL, Langerin) as calculated *via* SPR using the Langmuir 1 : 1 binding model

Lectin	Code	$k_a$ ( $\text{M}^{-1} \text{s}^{-1}$ )	$k_d$ ( $\text{s}^{-1}$ )	$K_d$ (M)	$R_{\text{max}}$ (RU)
DC-SIGN	<b>GP1</b>	387	$6.51 \times 10^{-4}$	$1.59 \times 10^{-6}$	3000
DC-SIGN	<b>GP2</b>	198	$3.39 \times 10^{-4}$	$1.72 \times 10^{-6}$	725
DC-SIGN	<b>GP3</b>	274	$2.71 \times 10^{-4}$	$9.88 \times 10^{-7}$	750
DC-SIGN	<b>GP4</b>	834	$8.08 \times 10^{-4}$	$9.69 \times 10^{-7}$	170
DC-SIGN	<b>GP5</b>	261	$6.57 \times 10^{-4}$	$2.52 \times 10^{-6}$	75
Langerin	<b>GP1</b>	14.2	$3.49 \times 10^{-5}$	$2.46 \times 10^{-6}$	430
Langerin	<b>GP2</b>	1220	$5.80 \times 10^{-4}$	$4.75 \times 10^{-7}$	110
Langerin	<b>GP3</b>	836	$2.80 \times 10^{-4}$	$3.43 \times 10^{-7}$	75
Langerin	<b>GP4</b>	1030	$2.82 \times 10^{-4}$	$2.73 \times 10^{-7}$	45
Langerin	<b>GP5</b>	2470	$9.23 \times 10^{-4}$	$3.73 \times 10^{-7}$	45
MBL	<b>GP1</b>	217	$1.42 \times 10^{-4}$	$6.54 \times 10^{-7}$	6500
MBL	<b>GP2</b>	84.3	$15.3 \times 10^{-4}$	$18.2 \times 10^{-6}$	205
MBL	<b>GP3</b>	172	$13.8 \times 10^{-4}$	$8.03 \times 10^{-6}$	140
MBL	<b>GP4</b>	470	$19.7 \times 10^{-4}$	$4.20 \times 10^{-6}$	140
MBL	<b>GP5</b>	307	$16.1 \times 10^{-4}$	$5.26 \times 10^{-6}$	100

copolymer structures were selected in order to keep the carbohydrate content constant, and a stock solution used to keep the first block consistent throughout the class. This was important so that we could accurately confirm that it was the molar mass influence that was affecting the binding affinity and not the increasing sugar content. Azide–alkyne end-group functionality was used for the ability to further functionalise if desired keeping the study relevant within the current literature.<sup>4,13</sup>

## Synthesis and analysis of glycopolymers **GP1–GP5**

Glycosylation of all the polymers was achieved *via* the post-polymerisation of the pendent double bonds. These were functionalised *via* a ‘thiol click’ reaction using  $\beta$ -thioglucose tetraacetate. The reaction was set up according to the following conditions: ene/thiol/V601 = 1.0/1.2/0.25. Completion of the glycosylation was monitored by  $^1\text{H}$  NMR (Fig. 2) *via* the disappearance of the allylic peak observed at 5.7 ppm. Subsequent addition of V601 and  $\beta$ -thioglucose tetraacetate was added if the allylic peak was still observed after 24 hours. After the completion of all ‘thiol–ene click’ reactions, the pendant sugars were deacetylated with NaOMe and the crude product dialysed against water to remove any remaining impurities. The dialysis cut off was 500–1000 Da and as a result likely removed some of the smaller chains, resulting in a narrower dispersity (Table 1 and Fig. 1).

The final glycopolymers were analysed *via* GPC (Fig. 1(B)), Fourier transform infrared spectroscopy (FT-IR) (Fig. S29–S36<sup>†</sup>) and  $^1\text{H}$  NMR (Fig. 2 and Fig. S19–S22<sup>†</sup>) were used to confirm complete deacetylation. The deacetylation was confirmed by the disappearance of the acetyl peaks at  $\sim 2.0$  ppm. This was also confirmed by FT-IR, the FT-IR was taken before and after deacetylation. After deacetylation the acetyl peaks ( $1600 \text{ cm}^{-1}$ ) disappeared and the broad OH peaks grew ( $3000 \text{ cm}^{-1}$ ). The glycopolymers **GP1–GP5** showed a difference between  $M_{n, \text{theo}}$  (calculated from conversion) and  $M_{n, \text{GPC}}$ . This result is likely due to the difference between the hydrodynamic volume of the standards used to calibrate the GPC, and the glycopolymer.

## Lectin binding analysis *via* SPR

SPR studies were conducted by immobilising lectins on a chip surface (CM5) and then flowing **GP1–GP5** over the substrate with a HBS buffer solution containing calcium (pH = 7.4). The binding assays were recorded in a concentration range of  $20 \mu\text{M}$ – $1.75 \mu\text{M}$ . The lectins used, MBL, DC-SIGN and Langerin, were all selected for their affinity towards glycosyl residues and their roles within the human innate immune response.<sup>48</sup>

It was expected that across the series, the binding affinity towards lectins would increase as molar mass increased due to the mass effect.<sup>49,50</sup> A general trend in affinity throughout the series was observed. Kinetic evaluation of SPR results suggests that overall, there is an increasing affinity with higher molar mass. After **GP4**, it seemed to reach a plateau, whereby after **GP4** the binding no longer increases rather it stays the same or decreases which agrees with the literature, whereby they increased the molar mass by increasing the sugar content.<sup>46</sup> It appears likely that these findings are caused by the increase in non-glycosylated polymer domains across the series, preventing the carbohydrates from reaching the lectin binding sites by coil formation. **GP1** demonstrated a large  $R_{\text{max}}$  value, likely due to the high density of carbohydrate in comparison to the other glycopolymers. It was observed that in all lectins that the  $R_{\text{max}}$  value decreased as the molar mass increased.



MBL is a type of lectin within human serum, which has a range of roles within the immune system. MBL is key to the innate immune response that can bind to pathogens and other invading pathogens to activate an antibody response

required for the removal of infection.<sup>51</sup> Glycopolymers **GP1**–**GP5** showed binding to MBL evidenced by the  $k_a$  values (Table 2) obtained from SPR. **GP1** has a  $K_d$  value of  $6.54 \times 10^{-7}$  M for MBL. This demonstrates that **GP1** has the strongest

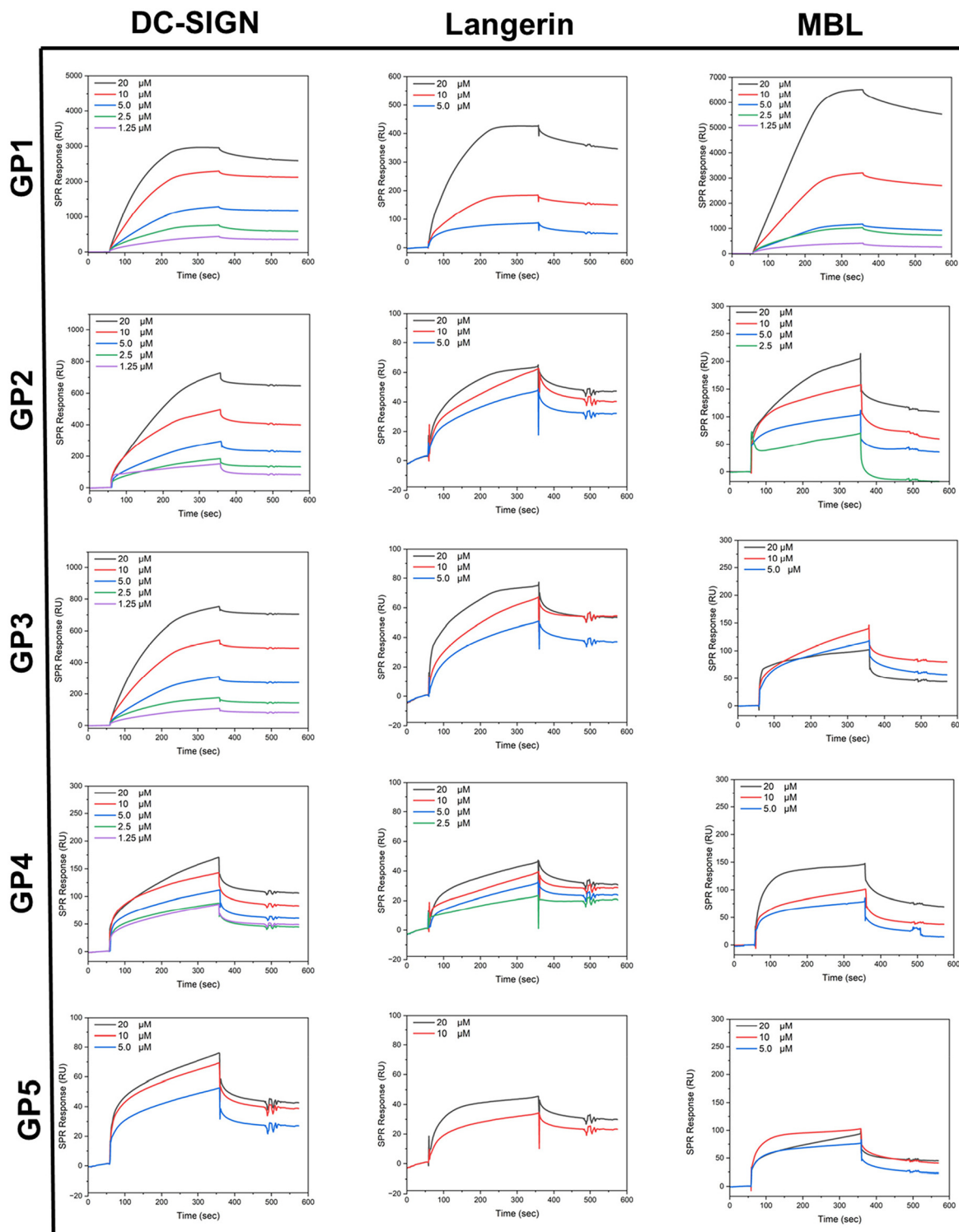


**Fig. 3** The SPR sensorgrams of glycopolymers **GP1**–**GP5** demonstrating the binding curves associated with them. All SPR measurements were carried out in a HBS buffer against immobilised lectins: DC-SIGN, Langerin and MBL.



binding within the class, further supported by its small  $k_d$  value of  $1.42 \times 10^{-4} \text{ s}^{-1}$ . This low dissociation rate constant indicated that strong interactions with the glucose units on **GP1** are persistent or that rebinding of released glucose units occurs more quickly than the dissociation of the complex during the buffer wash period. In comparison to the rest of the class, the  $R_{\text{max}}$  of **GP1** was  $\sim 10$  times greater whilst its affinity to the lectin (reflected by the  $k_d$  values) was  $\sim 100$  times greater than **GP2** and  $\sim 10$  times greater than the rest of the class. Overall, the kinetic values support that there is a maximum affinity in this series of polymers, as evidenced by the similar  $K_d$  values in **GP3–GP5**.

DC-SIGN is a C-type (calcium-dependent) transmembrane protein found predominantly in dendritic cells. DC-SIGN is a cell adhesion and pathogen recognition receptor, which has high affinity for mannose containing glycoproteins. Predominantly, DC-SIGN acts as an adhesion molecule but can also initiate the innate immune response.<sup>52</sup> All glycopolymers (**GP1–GP5**) demonstrated binding to DC-SIGN, as reflected by the  $k_a$  values and the SPR curves (Table 2 and Fig. 3). **GP4** was found to have the lowest  $K_d$  value of  $9.69 \times 10^{-7} \text{ M}$ , indicating that it binds the most effectively within the class to DC-SIGN, because of its slow disassociation. It should be noted that **GP1** has the highest  $R_{\text{max}}$  value within the class, and this also follows the previous trend observed of the glycopolymers binding to MBL. **GP5** demonstrated the weakest binding within the class. As discussed above, this is to be expected as polymer chains likely coil which restricts access to the pendant sugar moieties. Notably, all polymers, except for higher molar mass ones, displayed a saturated binding profile during the association phase, indicating that some lectin binding sites remained unoccupied on the chip. This could be attributed to the limited accessibility and flexibility of the carbohydrates on the polymer chain due to their bulky nature in solution.

Langerin is a transmembrane protein which binds specifically towards mannose, fucose and *N*-acetylglucosamine. Langerin is expressed in the Langerhans cells (LC) which are a subset of DC cells. Langerin, like other C-type lectins, are pattern recognition receptors which recognise carbohydrates expressed by pathogens.<sup>53</sup> All glycopolymers (**GP1–GP5**) demonstrated a reasonable binding to Langerin. This is confirmed by the  $k_a$  values (Table 2). **GP4** was found to have the greatest binding reflected by the lowest  $K_d$  value of  $2.73 \times 10^{-7} \text{ M}$ . Again, **GP1** had the highest  $R_{\text{max}}$  value within the class. This result follows the trend observed in the last two analysed lectins. In conclusion, as the molar mass increases the affinity increases up to a certain point. This point is the critical point at which the polymers with higher molar mass at constant glucose content likely block their own availability, reducing their binding capability.

Further investigations into **GP1** and its high  $R_{\text{max}}$  values were conducted *via* DLS in both water and buffer and TEM (Fig. 4). It should be noted that  $R_{\text{max}}$  has no direct influence on the binding efficacy of the polymer. However, it can be linked to the mass of the polymer.<sup>54</sup> This determined that **GP1** self-assembled into elongated micelle morphology (Fig. 4A).

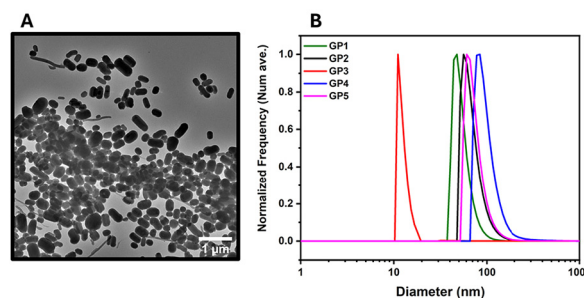


Fig. 4 The DLS and TEM of glycopolymers **GP1–GP5**. (A) TEM image of **GP1**. (B) The DLS traces of the glycopolymers **GP1–GP5** in an HBS buffer.

This feature was not observed in the other glycopolymers. The reason for the self-assembly could be attributable to hydrophobic nature of the butyl side chain. In theory this is sufficiently hydrophobic to act as a driving force for the self-assembly of **GP1**.

## Conclusions

In conclusion, we have demonstrated how the molar mass of glycopolymers influences their lectin binding. Initially, it was hypothesised that the polymers within the class would demonstrate increasing affinity as the molar mass increased even with the constant carbohydrate content. It was concluded that with increasing molar mass, the binding affinity did also increase up to a maximum point. With the maximum point possibly owing to the steric hindrance caused reduced availability of glucose units on the polymers. While all polymer parameters play a role in forming high affinity interactions, polymer length and epitope density are critical properties for developing effective glycopolymers against C-type human lectins.

Overall, a set of poly(2-oxazolines) copolymers was synthesised and subsequently glycosylated *via* thiol-ene chemistry. The resulting glycopolymers were successfully investigated by SPR and their affinities to three biologically relevant lectins was obtained. Thus, these glycopolymers not only investigate the impact of molar mass on their multivalent binding properties but also deepen our fundamental understanding of carbohydrate-lectin interactions in biological systems.

## Author contributions

C. R. B conceived the project. C. R. B and C. N. designed the experiments. C. N. conducted all experimental work. G. Y. helped perform SPR. J. L. did the TEM and DLS. Both J. L. and Z. V. supervised and discussed any problems associated with the project. All authors analysed the experimental data, edited, and commented on the manuscript.



## Data availability

The data supporting this article have been included as part of the ESI.†

## Conflicts of interest

There are no conflicts to declare.

## Acknowledgements

The authors are grateful for the Polymer RTP for analysis of polymers and EUTOPIA for providing funding for CN.

## References

- M. H. Stenzel, *Macromolecules*, 2022, **55**, 4867–4890.
- T. Zhao, R. Terracciano, J. Becker, A. Monaco, G. Yilmaz and C. R. Becer, *Biomacromolecules*, 2022, **23**, 543–575.
- S. S. Pinho, I. Alves, J. Gaifem and G. A. Rabinovich, *Cell. Mol. Immunol.*, 2023, **20**, 1101–1113.
- J. Becker, R. Terracciano, G. Yilmaz, R. Napier and C. R. Becer, *Biomacromolecules*, 2023, **24**, 1924–1933.
- T. E. Pauline, M. Rudd, P. Cresswell, I. A. Wilson and R. A. Dwek, *Science*, 2001, **291**, 2370–2376.
- Y. van Kooyk and G. A. Rabinovich, *Nat. Immunol.*, 2008, **9**, 593–601.
- B. Lepenies and R. Lang, *Front. Immunol.*, 2019, **10**, 2379–2382.
- L. Zheng, Y. Luo, K. Chen, Z. Zhang and G. Chen, *Biomacromolecules*, 2020, **21**, 5233–5240.
- X. Yan, A. Sivignon, N. Yamakawa, A. Crepet, C. Travelet, R. Borsali, T. Dumych, Z. Li, R. Bilyy, D. Deniaud, E. Fleury, N. Barnich, A. Darfeuille-Michaud, S. G. Gouin, J. Bouckaert and J. Bernard, *Biomacromolecules*, 2015, **16**, 1827–1836.
- U. I. M. Gerling-Driessen, M. Hoffmann, S. Schmidt, N. L. Snyder and L. Hartmann, *Chem. Soc. Rev.*, 2023, **52**, 2617–2642.
- M. Korpidou, J. Becker, S. Tarvirdipour, I. A. Dinu, C. R. Becer and C. G. Palivan, *Biomacromolecules*, 2024, **25**, 4492–4509.
- F. Demir Duman, A. Monaco, R. Foulkes, C. R. Becer and R. S. Forgan, *ACS Appl. Nano Mater.*, 2022, **5**, 13862–13873.
- G. Hayes, B. Dias-Barbieri, G. Yilmaz, R. J. Shattock and C. R. Becer, *Biomacromolecules*, 2023, **24**, 5142–5151.
- A. K. Blakney, R. Liu, G. Yilmaz, Y. Abdouni, P. F. McKay, C. R. Bouton, R. J. Shattock and C. R. Becer, *Polym. Chem.*, 2020, **11**, 3768–3774.
- M. Nagao, Y. Fujiwara, T. Matsubara, Y. Hoshino, T. Sato and Y. Miura, *Biomacromolecules*, 2017, **18**, 4385–4392.
- Y. Terada, A. Obara, H. Takamatsu, W. V. Espulgar, M. Saito and E. Tamiya, *ACS Appl. Bio Mater.*, 2021, **4**, 7913–7920.
- Y. Miura, Y. Hoshino and H. Seto, *Chem. Rev.*, 2016, **116**, 1673–1692.
- Y. Oz, Y. Abdouni, G. Yilmaz, C. R. Becer and A. Sanyal, *Polym. Chem.*, 2019, **10**, 3351–3361.
- G. Yilmaz, E. Guler, C. Geyik, B. Demir, M. Ozkan, D. Odaci Demirkol, S. Ozcelik, S. Timur and C. R. Becer, *Mol. Syst. Des. Eng.*, 2018, **3**, 150–158.
- J. J. Lundquist and E. J. Toone, *Chem. Rev.*, 2002, **102**, 555–578.
- J. Chen, R. Terracciano, J. Becker, G. Yilmaz and C. R. Becer, *Eur. Polym. J.*, 2024, **211**, 113006.
- M. Hartweg, Y. Jiang, G. Yilmaz, C. M. Jarvis, H. V. T. Nguyen, G. A. Primo, A. Monaco, V. P. Beyer, K. K. Chen, S. Mohapatra, S. Axelrod, R. Gómez-Bombarelli, L. L. Kiessling, C. R. Becer and J. A. Johnson, *JACS Au*, 2021, **1**, 1621–1630.
- A. Monaco, V. P. Beyer, R. Napier and C. R. Becer, *Biomacromolecules*, 2020, **21**, 3736–3744.
- Y. Abdouni, G. Yilmaz, A. Monaco, R. Aksakal and C. R. Becer, *Biomacromolecules*, 2020, **21**, 3756–3764.
- F. Shamout, A. Monaco, G. Yilmaz, C. R. Becer and L. Hartmann, *Macromol. Rapid Commun.*, 2020, **41**, 1900459.
- Y. Wang, Y. Kotsuchibashi, Y. Liu and R. Narain, *ACS Appl. Mater. Interfaces*, 2015, **7**, 1652–1661.
- G. Yilmaz, V. Uzunova, M. Hartweg, V. Beyer, R. Napier and C. R. Becer, *Polym. Chem.*, 2018, **9**, 611–618.
- Y. Chen, M. S. Lord, A. Piloni and M. H. Stenzel, *Macromolecules*, 2015, **48**, 346–357.
- F. Shamout, A. Monaco, G. Yilmaz, C. R. Becer and L. Hartmann, *Macromol. Rapid Commun.*, 2020, **41**, e1900459.
- G. Yilmaz, V. Uzunova, R. Napier and C. R. Becer, *Biomacromolecules*, 2018, **19**, 3040–3047.
- M. Bauer, C. Lautenschlaeger, K. Kempe, L. Tauhardt, U. S. Schubert and D. Fischer, *Macromol. Biosci.*, 2012, **12**, 986–998.
- T. Lorson, M. M. Lubtow, E. Wegener, M. S. Haider, S. Borova, D. Nahm, R. Jordan, M. Sokolski-Papkov, A. V. Kabanov and R. Luxenhofer, *Biomaterials*, 2018, **178**, 204–280.
- S. Zalipsky, C. B. Hansen, J. M. Oaks and T. M. Allen, *J. Pharm. Sci.*, 1996, **85**, 133–137.
- R. Hoogenboom and H. Schlaad, *Polymers*, 2011, **3**, 467–488.
- L. Yang, F. Wang, P. Ren, T. Zhang and Q. Zhang, *Macromol. Res.*, 2023, **31**, 413–426.
- C. J. Waschinski and J. C. Tiller, *Biomacromolecules*, 2005, **6**, 235–243.
- B. Verbraeken, B. D. Monnery, K. Lava and R. Hoogenboom, *Eur. Polym. J.*, 2017, **88**, 451–469.
- T. X. Viegas, M. D. Bentley, J. M. Harris, Z. Fang, K. Yoon, B. Dizman, R. Weimer, A. Mero, G. Pasut and F. M. Veronese, *Bioconjugate Chem.*, 2011, **22**, 976–986.
- R. Hoogenboom, *Eur. Polym. J.*, 2022, **179**, 111521–111531.



- 40 R. W. Moreadith, T. X. Viegas, M. D. Bentley, J. M. Harris, Z. Fang, K. Yoon, B. Dizman, R. Weimer, B. P. Rae, X. Li, C. Rader, D. Standaert and W. Olanow, *Eur. Polym. J.*, 2017, **88**, 524–552.
- 41 M. Lu, Y. Y. Khine, F. Chen, C. Cao, C. J. Garvey, H. Lu and M. H. Stenzel, *Biomacromolecules*, 2019, **20**, 273–284.
- 42 J. Leong, J. Y. Teo, V. K. Aakalu, Y. Y. Yang and H. Kong, *Adv. Healthc. Mater.*, 2018, **7**, 1701276–1701303.
- 43 K. H. M. Motomu Kanai and L. L. Kiessling, *J. Am. Chem. Soc.*, 1997, **119**, 9931–9932.
- 44 S. J. Richards and M. I. Gibson, *JACS Au*, 2021, **1**, 2089–2099.
- 45 M. Ahmed and R. Narain, *Biomaterials*, 2012, **33**, 3990–4001.
- 46 K. Lin and A. M. Kasko, *Biomacromolecules*, 2013, **14**, 350–357.
- 47 A. V. Anja Gress and H. Schlaad, *Macromolecules*, 2007, **40**, 7928–7933.
- 48 C. D. Raposo, A. B. Canelas and M. T. Barros, *Biomolecules*, 2021, **11**, 188–215.
- 49 S. G. Patching, *Biochim. Biophys. Acta*, 2014, **1838**, 43–55.
- 50 R. P. Sparks, J. L. Jenkins and R. Fratti, *Methods Mol. Biol.*, 2019, **1860**, 199–210.
- 51 M. W. Turner, *Immunobiology*, 1998, **199**, 327–339.
- 52 Y. van Kooyk and T. B. Geijtenbeek, *Nat. Rev. Immunol.*, 2003, **3**, 697–709.
- 53 M. van der Vlist and T. B. Geijtenbeek, *Immunol. Cell Biol.*, 2010, **88**, 410–415.
- 54 N. J. de Mol and M. J. E. Fischer, *Surface Plasmon Resonance: A General Introduction*, Springer, New York, 2010.

